J Appl Electrochem (2010) 40:1281–1291
DOI 10.1007/s10800-010-0077-y

ORIGINAL PAPER

Photoelectrocatalysis reactivity of independent titania nanotubes

Yibing Xie · Degang Fu

Received: 3 September 2009 / Accepted: 9 January 2010 / Published online: 22 January 2010

Abstract Two types of independent titania nanotube arrays with the separated tube wall structure have been fabricated by a controlled anodization process and used for photoelectrocatalysis (PEC) applications. The photocatalysis degradation efficiency of the organic pollutant is improved from 6.0 to 9.2% through increasing tube length and inter-tube space. The PEC degradation efficiency is 20.4% at an applied potential of 2.885 V for titania long nanotube array. An electro-Fenton-assisted PEC reaction system has been developed using titania long nanotube array and an iron sheet as two anodes in a parallel connection and a multiporous carbon as one cathode. The current distribution among three functional electrodes is conducted to optimize titania PEC reaction and electro-Fenton reaction. Accordingly, the degradation efficiency is improved from 20.4% in PEC to 60.2% in electro-Fenton-assisted PEC, and the mineralization efficiency is also improved from 8.1 to 37.4%. The corresponding reaction rate constant of 5.19×10^{-3} min^{-1} is even higher than that of 3.98×10^{-3} min^{-1} for the sum of individual oxidation reactions of titania PEC, electro-Fenton, and anodic electrolysis.

Keywords Titania · Independent nanotubes · Photoelectrocatalysis · Electro-Fenton · Degradation

Y. Xie (✉)
School of Chemistry and Chemical Engineering, Southeast University, Nanjing, China
e-mail: ybxie@seu.edu.cn

D. Fu
State Key Laboratory of Bioelectronics, Southeast University, Nanjing, China

1 Introduction

In the area of environmental purification and remediation, many advanced oxidation technologies have been developed to degrade various organic pollutants [1–3]. Both photochemical oxidation utilizing a photon energy to achieve a target chemical reaction and electrochemical oxidation using an electrical energy to drive a desired chemical reaction have been developed to act as complementary technologies of a conventional biological process for environmental decontamination. UV light or visible light-induced photocatalysis oxidation processes have been widely investigated for degrading organic pollutants in aqueous solution. Various electrochemical oxidation processes, such as anodic electrolysis, electro-Fenton and photo-assisted electron-Fenton, have also been developed using functional anodes and cathodes [4, 5]. The advantages of such electrochemical technologies include low cost of electricity compared to chemical oxidation technology and using only electrons as reagents. The high reactivity of Fenton reaction makes it suitable and effective for degrading environmental pollutants. In the photochemical oxidation, titania (TiO_2) can act as a very effective photocatalyst for non-selective oxidation and mineralization of various organic pollutants under UV light illumination. TiO_2 photocatalysis and photoelectrocatalysis (PEC) processes have been widely investigated for water treatment applications [6–9]. Porous TiO_2 film electrodes with the desired morphologies have been synthesized by anodizing Ti metal in different electrolyte solutions [10–12]. It is proved that highly ordered TiO_2 nanotube arrays exhibit higher photocatalysis efficiency in organic pollutant degradation than the TiO_2 nanoparticle films [13–15]. Such photocatalysis activity can be further improved by adjusting TiO_2 morphology from the interconnected nanotube

walls to the separated ones because the mass and charge transfer can be promoted [16]. It is also reported that inherent photocatalytic activity of TiO_2 nanotube array can be improved by chemical doping and microstructure modifications [14, 17, 18]. However, TiO_2 heterogenerous photocatalysis still has a very low rate of electron transfer from the TiO_2 conduction band to oxygen molecules and a high rate of recombination between the photogenerated electrons and holes. Thus, this process has a low quantum efficiency below 5% [19]. Recently, both electro-assisted and peroxide hydrogen (H_2O_2)-assisted TiO_2 photocatalysis oxidation processes have been developed as an effective approach to enhance photocatalytic degradation efficiency of organic pollutants [20, 21].

In this study, independent and free-standing TiO_2 nanotube arrays with the separated tube wall structure will be fabricated to act as a photocatalyst as well as a photoanode. Microstructure modification of TiO_2 nanotubes is expected to improve the photocatalysis reactivity. A photo-electro-assisted oxidation reaction system that includes both electrochemical oxidation and photochemical oxidation in an integrated process has been developed using multi-electrode configuration. In our previous study, Fenton-assisted PEC of TiO_2 microporous film can be well established using two functional electrodes of the TiO_2 photoanode and carbon (C) cathode. H_2O_2 is electrically generated on the carbon electrode and ferrous ion (Fe^{2+}) is chemically dosed into the solution [22, 23]. In this study, an electro-Fenton-assisted PEC will be established using three functional electrodes, namely TiO_2 photoanode, Fe anode, and carbon cathode. Both H_2O_2 and Fe^{2+} can be electrically generated on individual electrode. Such photo-electro-assisted oxidation system is expected to have the enhanced PEC reactivity of TiO_2 nanotube array.

2 Experimental

2.1 Material preparation

TiO_2 nanotube array was synthesized by a potentiostatic anodization process. The electrochemical preparation experiment was carried out in a cylindrical polyflon reactor equipped with a dc power source (Agilent 6634B) and a two-electrode configuration. A titanium sheet (Ti, purity of 99.6%, thickness of 0.2 mm, Strem Chemicals, Inc., Newburyport, USA) is used as an anode and a platinum sheet (Pt, purity of 99.95%, thickness of 0.05 mm, Sigma–Aldrich, St. Louis, USA) is used as a cathode. The Ti sheet was pretreated by ultrasonic cleaning in acetone and alcohol solution for 20 min. A chemical polishing process was then carried out in a mixed acid solution with 3.3 M HF and 5.6 M HNO_3 for 15 s to form a fresh Ti metal with a planar surface. After that, an anodic oxidation of Ti metal was conducted at 30 V for 2 h in ethylene glycol/water (volume ratio, 40/60) mixture solution with 0.4 M H_3PO_4 and 0.15 M HF electrolyte. Alternatively, another anodization process was conducted at 60 V for 8 h in ethylene glycol solution with 0.20 M H_2O, 0.4 M H_3PO_4, and 0.15 M NH_4F electrolyte. Finally, the annealing treatment was conducted at 200, 450, and 600 °C for 2 h in air atmosphere for the crystal structure investigation of anodic TiO_2.

2.2 Experimental setup and procedure

The experimental setup for the electro-Fenton-assisted TiO_2 PEC reaction system is illustrated in Fig. 1. A cylindrical quartz glass cell with an effective vessel volume of 80 mL was used as a photoelectrochemical reactor. TiO_2 nanotube photoelectrode was vertically placed in a reaction solution close to its inner wall of the quartz cell reactor. An 8-W medium-pressure mercury lamp with a main emission wavelength of 365 nm and irradiation intensity of 0.68 mW cm^{-2} was used as a UV light source to irradiate TiO_2 photoelectrode. The whole UV lamp having a parabolic trough configuration was placed on the outer surface of the quartz cell reactor. The distance between UV lamp and TiO_2 photoelectrode was about 15 mm.

The TiO_2 nanotube array grown on the Ti sheet (TiO_2/Ti) with a size of 10 × 50 × 0.2 mm was used as one anode. A piece of rectangle stainless steel sheet with a size of 10 × 50 × 1 mm was used as the iron (Fe) anode. It previously conducted an electrochemical pretreatment in nitric acid, sulfuric acid, and perchloric acid solution to form a surface passive film [24]. A reticulated vitreous carbon foam (C, size of 10 × 50 × 5 mm, bulk density of 1.54 g cm^{-3}, bulk resistivity of 0.05 ohm cm^{-1}, ERG Corp., Oakland, USA) was used as a multiporous carbon electrode. A variable electrical resistor and Fe electrode were connected in series. Meanwhile, TiO_2 and Fe electrodes were connected in parallel. The current distribution between them is adjusted by the variable electrical resistor. Herein, the TiO_2 electrode was used as a photoanode to conduct PEC oxidation reaction under UV light illumination. The Fe electrode was used as another anode to release ferrous ion (Fe^{2+}). The variable electrical resistor was used to adjust current distribution between TiO_2 and Fe anodes. Multiporous carbon was used as a cathode to generate H_2O_2 continuously. Electro-Fenton oxidation reaction was established between electrogenerated H_2O_2 and Fe^{2+}. A saturated calomel electrode (SCE) was also placed in a separate chamber to control the electrode potential of the TiO_2 photoanode. The potential and current of the working electrode were controlled by a potentiostat–galvanostat.

Orange G (OG, $C_{16}H_{10}N_2O_7S_2Na_2$, reagent grade purity of 86%, Sigma Chemical, St. Louis, USA) was used as the

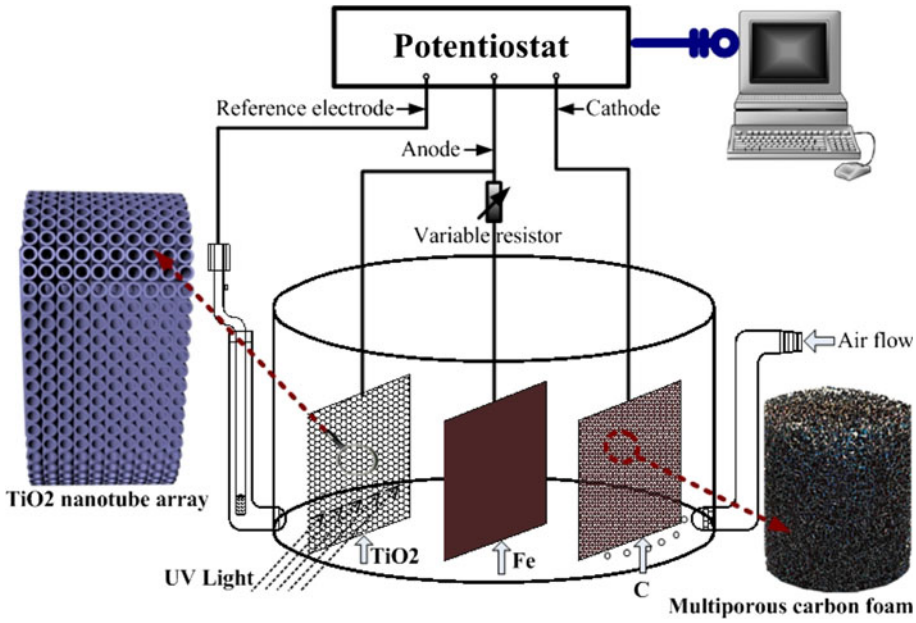

Fig. 1 Schematic diagram of photo-electro-assisted reaction system with TiO_2–Fe–C multi-electrode configuration

model pollutant without further purification. All degradation experiments were conducted in 0.1 mM OG aqueous solution. Air was continuously supplied into this aqueous solution with an air flow of 120 mL min^{-1}. A sodium sulfate solution (Na_2SO_4, 0.01 M) was used as a supporting electrolyte in the OG solution. The initial pH was found to be 6.1 and was not controlled during the whole reaction. The multiporous carbon electrode can adsorb OG on its surface. Prior to reaction, all electrodes were immersed in 0.1 mM OG solution for 120 min to reach an adsorption/desorption equilibrium.

2.3 Characterization and analysis method

A field emission scanning electron microscope (FESEM, JEOL JSM-6335F) was used to investigate the surface morphology and microstructure of as-prepared TiO_2. An X-ray diffractometer (XRD, Philips PW3020) fitted with a graphite monochromator was used to determine the crystallinity of TiO_2. All electrochemical measurements were conducted in 0.01 M Na_2SO_4 solution. Using an electrochemical workstation (IM6e, Zahner Elektrik) and a three-electrode configuration that consists of TiO_2 sheet as a working electrode, Pt sheet as a counter electrode and an SCE as a reference electrode. The OG concentration was determined by high performance liquid chromatography (HPLC, Agilent-1100) with a chromatography column (Agilent Extend-C18), a mobile phase of acetonitrile and water (volume ratio, 70/30) at a flowrate of 0.8 mL min^{-1}, and a UV detection wavelength at 478 nm. The retention time of OG peak was found to be 3.12 min in HPLC analysis. The dissolved organic carbon (DOC) concentration was measured by a total organic carbon analyzer (Shimadzu TOC-VCSN). The total dissolved iron ion concentration was measured by an atomic absorption spectrometer (AAnalyst 300, Perkin-Elmer, Waltham, USA) fitted with a graphite furnace (HGA-850).

3 Results and discussion

3.1 Microstructure characterization

FESEM images of anodic TiO_2 films are shown in Fig. 2. One type of TiO_2 directly grown on Ti substrate has a highly ordered and regularly aligned nanotube array structure. These nanotubes are mostly separated to form an independent arrangement structure. The interval space of nanotube walls is about tens of nanometer. Individual nanotube has open pore mouth with a mean size of 100 nm and wall thickness of 15 nm (see Fig. 2b). Cross section view shows that the total tube length is around 1.1 μm (see Fig. 2a). Comparatively, another type of TiO_2 also exhibits a highly ordered nanotube array structure. These nanotubes are completely separated from each other and have a much larger inter-pore distance, whose size is close to hundreds of nanometer (see Fig. 2c). Although a similar size of pore mouth and wall thickness has been obtained, the total tube length has increased up to 6.1 μm (see Fig. 2d). However, the uniform arrangement of the long nanotubes is inferior to that of the short nanotubes. Both types of TiO_2 nanotube arrays prepared by an anodic oxidation process are originated from Ti sheet. Such TiO_2 films have a high mechanical strength to tightly bond with Ti substrate. Such TiO_2 nanotube arrays could be more durable than other TiO_2 films prepared usually by a sol–gel process.

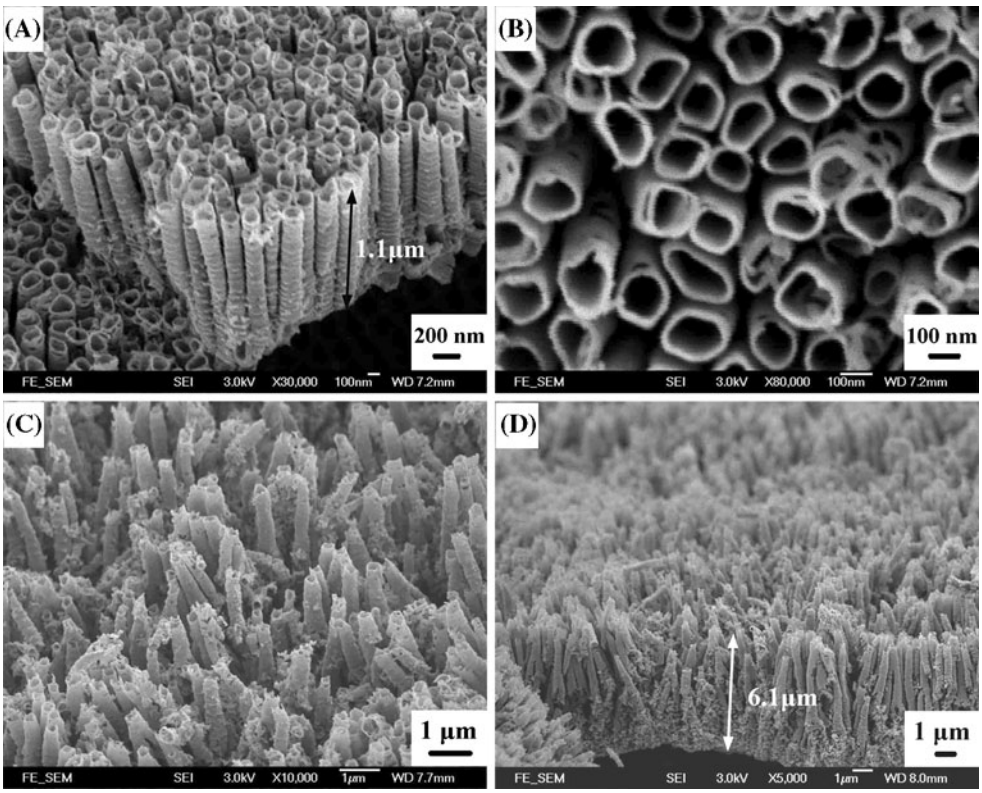

Fig. 2 FESEM images of TiO_2 nanotube array prepared by an anodization process and a heating treatment: (**a**) cross-section view and (**b**) top view of short nanotubes; (**c**) top view and (**d**) cross-section view of long nanotubes

Furthermore, independent TiO_2 nanotubes with a completely separated structure would be beneficial to interfacial adsorption of organic compounds on tube wall surface and therefore could promote a heterogeneous reaction. In this study, the TiO_2 long nanotube array with an enlarged inter-pore distance will be intensively investigated for photocatalysis and PEC applications.

XRD characterization has been carried out to investigate the crystallinity of TiO_2 long nanotube array that is annealed at different temperature. XRD patterns of all TiO_2/Ti samples have the characteristic diffraction peaks of Ti metal crystal due to the Ti electrode substrate (see Fig. 3). In particular, TiO_2 nanotube array without any heating treatment has an amorphous structure because the as-prepared TiO_2/Ti only displays the characteristic peaks of Ti metal crystal (curves a and b). Comparatively, the TiO_2 nanotube array with a heating treatment at 200 °C for 2 h has a primary anatase crystal structure due to the appearance of characteristic diffraction peaks at 25.4° of crystal plane (101) and 48.1° of crystal plane (200) (curve c). Even after a heating treatment at 450 °C for 2 h, this TiO_2 still keeps a sole anatase structure, but the diffraction peak intensity of crystal plane (101) has increased obviously (curve d). This means that the annealing treatment at a proper temperature can complete the crystallization process. However, after a heating treatment at 600 °C for 2 h, this TiO_2 sample reveals another new diffraction peak at 27.5° that is corresponding to the crystal plane (110) of rutile TiO_2 (curve e). Therefore, this kind of TiO_2 is composed of predominant anatase and minor rutile. It also indicates that the overheating treatment above 600 °C can cause TiO_2 nanotube array to accomplish a phase transfer from anatase to rutile structure. In general, the anatase TiO_2 exhibits a higher photocatalytic reactivity than the rutile one. In this study, all TiO_2 nanotube electrodes accordingly undergo a heating treatment at 450 °C for 2 h.

3.2 Electrochemical behavior

To better understand the electrochemical behavior of the TiO_2 long nanotube array, the linear sweep voltammetry curves are measured in 0.01 M Na_2SO_4 solution when the electrode potential is swept from −1.0 to 3.5 V versus SCE (see Fig. 4). Considering the polarization current curves of TiO_2 nanotube electrode under a dark condition, a sharp increase in the polarization current can be observed at a negative potential. This is due to the electrochemical reduction reaction of H_2O. The very small current profile observed at low anodic potentials above 0 V versus SCE is the typical characteristic of a passive TiO_2 film. However,

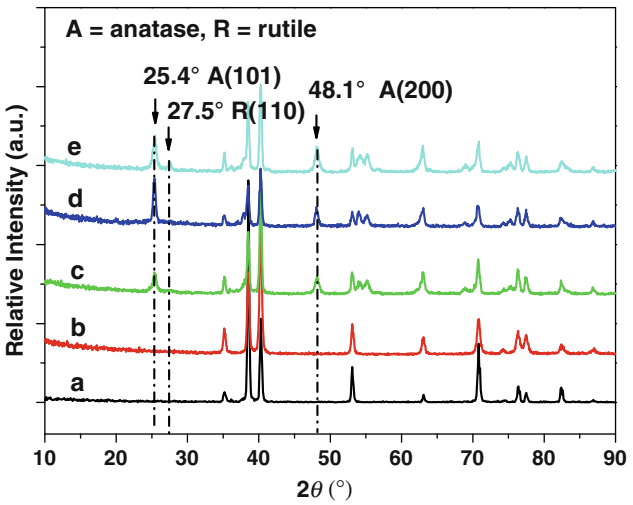

Fig. 3 XRD patterns of *a* bare Ti substrate; and TiO_2/Ti electrodes (*b*) without heating treatment, with annealing at *c* 200 °C, *d* 450 °C, *e* 600 °C for 2 h

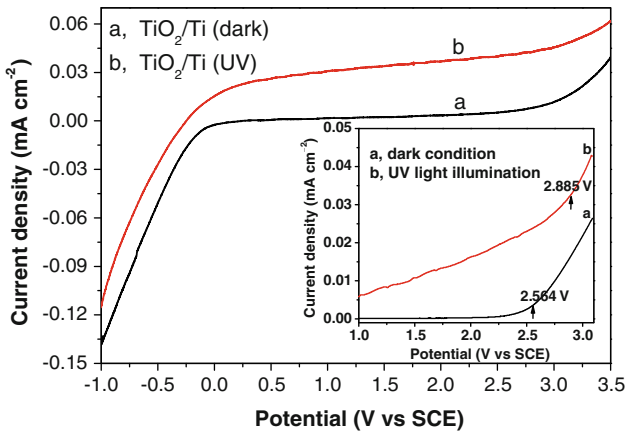

Fig. 4 Linear sweep voltammetry curves of TiO_2 long nanotube array in 0.01 M Na_2SO_4 solution under *a* a dark condition and *b* UV light illumination. The inset shows the enlarged voltammogram curves at the critical potential of TiO_2

this polarization current can quickly rise from 2.8 to 26 μA cm^{-2} when the applied potential is increased from 2.5 to 3.0 V. A drastic increase in polarization current at a higher potential above 2.6 V is due to the electrochemical oxidation reaction of H_2O. Meanwhile, a dissolution corrosion reaction of TiO_2 semiconductor must have occurred at a higher anodic potential. This voltammogram behavior can be well explained to the typical character of *n*-type semiconductor for anatase TiO_2 nanotube array. The polarization current is obviously higher under UV light illumination than that under a dark condition when the same anodic potential is applied on the TiO_2 photoelectrode. An applied anodic potential can promote the separation of photogenerated electron–hole pairs through an electron transfer from TiO_2 conduction band to the Ti substrate and then the counter electrode, resulting in an increase in polarization current. A critical breakdown potential is determined at the turning point of electrode current change. Its corresponding value is about 2.885 V under UV light illumination and 2.564 V under a dark condition for this TiO_2 long nanotube array (see inset of Fig. 4). This breakdown potential is still more positive than the theoretical value of valance band oxidation potential of TiO_2 that is only 2.458 V versus SCE ($E_{VB} = +2.7$ V versus NHE at pH 7) [19]. So, the critical polarization potential is not only determined by its inherent semiconductor property, but also dependent on crystal structure, crystallization degree, film thickness, and electrode electric field. In view of the polarization experiment, the applied anode potential of this TiO_2 nanotube photoelectrode should be below this anodic potential of 2.885 V (corresponding current density, 38 μA cm^{-2}) in a PEC reaction.

3.3 Photocatalysis and PEC

Both photocatalysis and electro-assisted photocatalysis (i.e., PEC) reactions are carried out for OG degradation on the base of two types of TiO_2 nanotube arrays. The degradation curves are shown in Fig. 5 and experimental results are listed in Table 1. The initial DOC concentration is 12.6 mg L^{-1} in 0.1 mM OG aqueous solution. The DOC removal ratio represents the mineralization efficiency of organic pollutants.

It has proven that the independent nanotubes have a higher photocatalytic activity than the interconnected nanotubes for organic pollutant degradation [16]. Herein, two types of independent TiO_2 nanotube arrays are used for photocatalysis degradation of a model pollutant of OG (see Fig. 5A). In the absence of any TiO_2 photocatalyst, the degradation ratio of OG is only less than 1.0% by a UV photolysis process for 180 min (curve a). In the TiO_2 photocatalysis, the degradation ratio is determined to be 6.0% for a short nanotube array with a small inter-pore distance and a length of 1.1 μm. It increases up to 9.6% for a long nanotube array with a large inter-pore distance and a length of 6.1 μm (curves b and c). This means that the photocatalysis degradation efficiency can be well improved through adjusting TiO_2 nanotube length and inter-tube space. The corresponding DOC removal ratio only increases from 4.6 to 6.3%, indicating an insignificant mineralization efficiency in above photocatalysis processes. Usually, the TiO_2 heterogeneous photocatalytic reaction is a diffusion-kinetics controlled process [25]. The long nanotubes with a separated tube wall structure can provide much more accessible surface area for mass and charge transfer. Therefore, the microstructure modification can enhance photocatalysis reactivity of TiO_2 nanotube array to a certain degree. In the following studies, the PEC

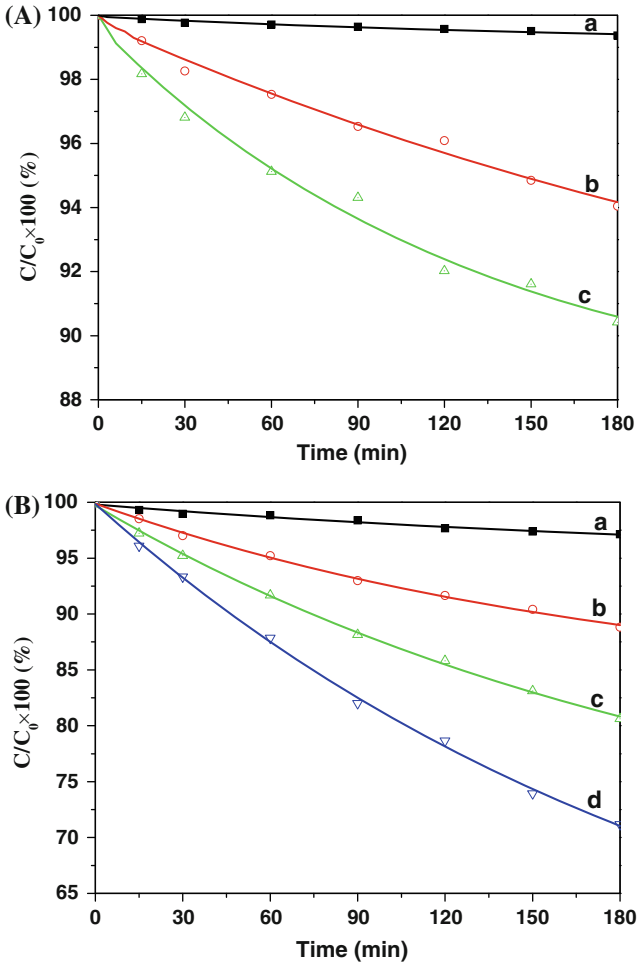

Fig. 5 OG degradation curves in (A) TiO_2 photocatalysis process *a* in the absence of TiO_2, *b* using TiO_2 short nanotube array, *c* using TiO_2 long nanotube array; and (B) TiO_2 PEC process under conditions of *a* TiO_2 current density of 38 mA cm^{-2} without UV light illumination, and TiO_2 current density of *b* 12 mA cm^{-2}, *c* 38 mA cm^{-2}, *d* 300 mA cm^{-2} under UV light illumination

reactivity of independent long nanotube array will be further investigated.

The PEC oxidation reaction is carried out for OG degradation to investigate the effect of current density of the TiO_2 photoanode. The corresponding degradation curves are shown in Fig. 5B. The anodic electrolysis of OG occurred on TiO_2 electrode under a dark condition causes a low degradation ratio of 2.8% (curve a). In a PEC process, when TiO_2 nanotube array electrode is applied an anode potential of 1.945 and 2.885 V, the corresponding current density is 12 and 38 μA cm^{-2}. The degradation ratio of OG is determined to be 11.2 and 20.4%, respectively (curves b and c). Therefore, the degradation ratio is increased by applying a controlled anodic potential on the TiO_2 photoelectrode. The PEC process behaves much higher degradation efficiency than photocatalysis process. It is well known that the anodic potential applied on TiO_2 electrode can suppress the recombination of photogenerated electron–hole pairs and then promote the degradation reaction of organic pollutants [26]. Such PEC reactivity of the TiO_2 photoanode can be further improved by increasing its electrode potential in a low potential range and then reach a steady level at a high potential stage. Table 1 shows that the PEC is more effective than photolysis, electrolysis and photocatalysis alone. The degradation efficiency of OG (degradation ratio, 20.4%) in such a PEC reaction is even higher than the sum (total degradation ratio, 15.2%) of individual electrochemical and photochemical processes. This result is ascribed to an interactive effect between photo-oxidation reaction and electro-oxidation reaction [27]. Furthermore, when the applied current density of the TiO_2 photoanode is highly increased up to 300 μA cm^{-2}, the degradation ratio of OG is accordingly increased up to 28.8% (curve d). However, under such high current condition, its corresponding potential of 12.8 V is much higher than the critical breakdown potential of 2.885 V for anatase TiO_2 semiconductor and this TiO_2 film electrode has suffered a dissolution reaction to destroy nanotubular film structure.

3.4 Electro-Fenton-assisted PEC

In order to further improve TiO_2 PEC reactivity, electro-Fenton-assisted PEC reaction system has been developed for organic pollutant degradation. Such a process mainly involves three oxidation reactions of TiO_2 PEC, electro-Fenton, and anodic electrolysis. TiO_2 nanotube array electrode only needs a low anodic potential to drive these

Table 1 OG degradation ratio and DOC removal ratio after 180 min in TiO_2 photocatalysis (PC) reaction system with a control of nanotube length and TiO_2 PEC reaction system with an anodic potential control of TiO_2–Pt electrode pair

Reaction condition	Photolysis	PC		Electrolysis	PEC		
	No TiO_2 + UV	Short TiO_2 + UV	Long TiO_2 + UV	2.885 V + No UV	1.945 V + UV	2.885 V + UV	12.852 V + UV
OG degradation ratio (%)	<1.0	6.0	9.6	2.8	11.2	20.4	28.8
DOC removal ratio (%)	0	4.6	6.3	0.8	7.4	8.1	12.3

electrons away via an external electrical circuit in a PEC reaction. Once the electrical potential exceeds its critical breakdown potential, TiO_2 nanotube array will suffer a dissolution process and gradually peel off from Ti substrate. On the other hand, the carbon electrode needs high electrical current density to generate sufficient H_2O_2 for electro-Fenton- and H_2O_2-assisted PEC oxidation reaction. Therefore, in this integrated reaction system, when a high current density on the carbon cathode is applied, the variable electrical resistor is used to distribute its minor fraction to the TiO_2 photoanode and major fraction to the Fe anode.

Three experiments are carried out in a photo-electro-assisted reaction system with TiO_2–Fe–C multi-electrode configuration and the controlled current distribution (see Fig. 6). The corresponding experimental results are listed in Table 2. The first experiment is performed under UV light illumination and a controlled current distribution (carbon cathode, 120 μA cm^{-2}; TiO_2 anode, 38 μA cm^{-2}; Fe anode, 130 μA cm^{-2}). OG degradation ratio and DOC removal ratio after 180 min are 60.2 and 37.4%, respectively (see curve c). This performance mainly results from three oxidation reactions including TiO_2 PEC, electro-Fenton, and anodic electrolysis. The second experiment is performed under a dark condition and a current control. The OG degradation ratio is determined to be 21.7%, which is caused by both electro-Fenton oxidation and anodic electrolysis oxidation (see curve a). Herein, the total cell current of 1.5 mA may not be high enough to carry out an effective anodic electrolysis oxidation on TiO_2 or Fe electrodes. OG degradation in this experiment results more from electro-Fenton oxidation rather than anodic electrolysis oxidation. The third experiment is conducted under UV light illumination, but without any current distribution between TiO_2 and Fe electrodes. The same cell current of 1.5 mA (current density, 120 μA cm^{-2}) is applied on the carbon electrode. Since the electrical resistance of TiO_2 electrode is much larger than that of Fe electrode, the TiO_2 electrode current is only 0.02 mA (current density, 4 μA cm^{-2}). This value is much less than Fe electrode current of 1.48 mA (current density, 148 μA cm^{-2}). OG degradation ratio and DOC removal ratio are 43.5 and 18.8%, respectively (see curve b). In comparison with the experimental result in curve c, the decrease in degradation efficiency is ascribed to the depressed PEC reaction that occurred on the TiO_2 photoanode under such a very low anodic current or potential condition. The obvious decrease in mineralization efficiency is due to the excessive releasing of ferrous ion into reaction solution. Therefore, it is necessary to balance each oxidation reaction to promote overall photoelectrochemical efficiency by controlling the current distribution among three functional electrodes in this photo-electro-assisted reaction system.

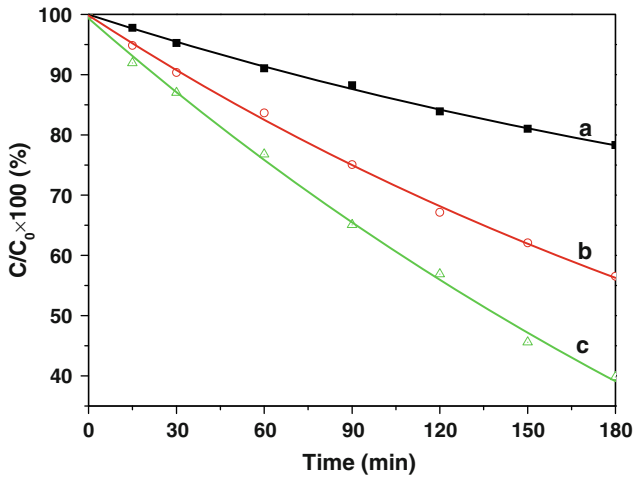

Fig. 6 OG degradation curves in a photo-electro-assisted reaction system with TiO_2–Fe–C multi-electrode configuration and a current control of *a* 38 μA cm^{-2} for TiO_2 and 130 μA cm^{-2} for Fe under a dark condition, *b* 4 μA cm^{-2} for TiO_2 and 148 μA cm^{-2} for Fe under UV light illumination, *c* 38 μA cm^{-2} for TiO_2 and 130 μA cm^{-2} for Fe under UV light illumination

Table 2 OG degradation ratio and DOC removal ratio after 180 min in a photo-electro-assisted reaction system with TiO_2–Fe–C multi-electrode configuration, current distribution, and UV light control

Reaction condition	No UV + current control	UV + no current control	UV + current control
OG degradation ratio (%)	21.7	43.5	60.2
DOC removal ratio (%)	16.2	18.8	37.4

3.5 Effect of electrogeneration H_2O_2 and ferrous ion

In general, H_2O_2 can be formed on multiporous carbon electrode through an electrochemical reduction reaction. The electrogeneration H_2O_2 mainly relies on the properties of electrode material, current density, oxygen coverage on the cathode, and pH value of electrolyte solution. Herein, the cumulative concentration of H_2O_2 has been investigated in a Pt–C electrode pair system with a cathode current control. The H_2O_2 concentration (c) in dependence on the electrolyzing time (t) and current density (I) is shown in Fig. 7. Obviously, a higher cathode current applied on the carbon electrode results in a higher H_2O_2 concentration in the solution. Herein, it is assumed that the electrogeneration reaction of H_2O_2 follows the first-order reaction kinetics and the generation rate of H_2O_2 is proportional to the current density of carbon cathode. An exponential model formula $c = [aI^*(1 - \exp(-k^*t)]$ can be applied to fit experimental data. The corresponding fitting curve

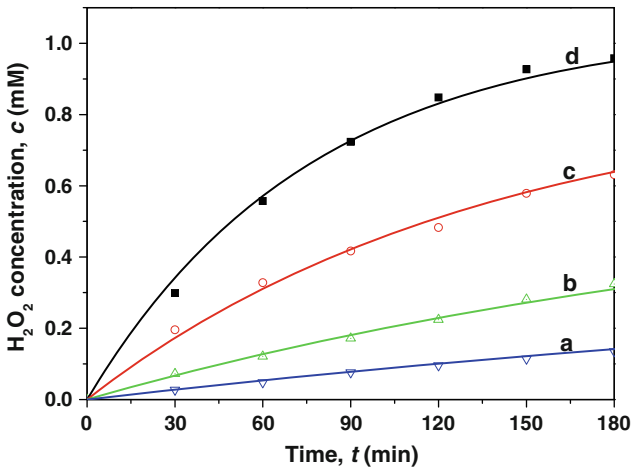

Fig. 7 Cumulative concentration of H_2O_2 electrogenerated on the carbon cathode with a current control of *a* 20 μA cm^{-2}, *b* 40 μA cm^{-2}, *c* 80 μA cm^{-2}, *d* 120 μA cm^{-2}

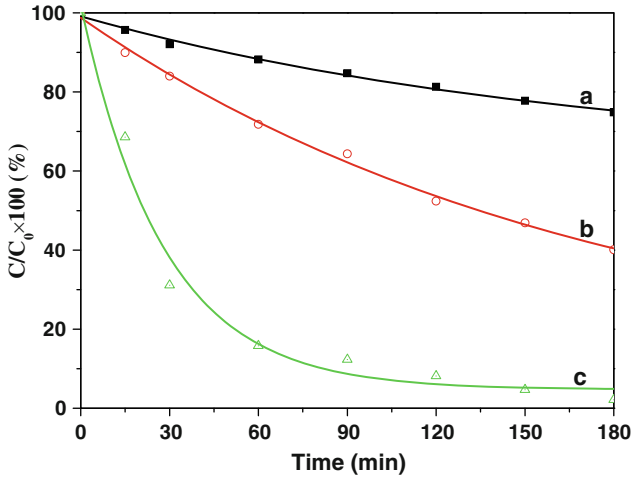

Fig. 8 OG degradation curves in a PEC process having the multi-electrode configuration with a current control: *a* TiO_2–Fe–Pt with a cell current of 1.5 mA, *b* TiO_2–Fe–C with a cell current of 1.5 mA, and *c* TiO_2–Fe–C with a cell current of 10 mA

formulas can be obtained as shown in Table 3. The linear relationship between the cumulative concentration of H_2O_2 and current density of carbon cathode can be obtained to estimate the practical concentration of electrogeneration H_2O_2 at different current densities. Accordingly, the fitting formula is obtained as $c = -0.0166 + 0.00813*I$.

Three experiments are conducted under critical conditions to investigate the effect of electrogeneration H_2O_2 on OG degradation efficiency. In the first experiment, the multiporous carbon electrode is replaced by a Pt electrode and the TiO_2–Fe–C electrode system becomes a TiO_2–Fe–Pt electrode system. None of H_2O_2 is electrochemically generated and OG is mainly degraded by both TiO_2 PEC oxidation and anodic electrolysis oxidation. In the other two experiments, TiO_2–Fe–C electrode system is still used and the current density of TiO_2 electrode remains at 38 μA cm^{-2}. However, the surface current density on the carbon electrode is increased from 120 to 800 μA cm^{-2} and the corresponding cell current is also increased from 1.5 to 10 mA. The concentration of electrogeneration H_2O_2 can be enhanced from 0.96 to 6.48 mM. The experimental results are shown in Fig. 8. The first experiment demonstrates that OG degradation ratio after 180 min is only 25.2% in the absence of electrogeneration H_2O_2 (see curve a). The other two experiments demonstrate that OG degradation ratio after 180 min is increased from 59.8 to 97.8% when more H_2O_2 is electrochemically generated by increasing current density of the carbon cathode (see curves b and c). In view of individual reaction efficiency under such high current condition, both electro-Fenton oxidation and anodic electrolysis oxidation can play a very important role for OG degradation. However, TiO_2 PEC oxidation becomes an insignificant process in this integrated oxidation reaction system. A slight flocculation phenomenon has been observed eventually because excessive ferrous ion has been electrochemically generated on the Fe electrode.

In general, ferrous ion plays a critical role in Fenton reaction as it influences the generation of hydroxyl radical ($Fe^{2+} + H_2O_2 \rightarrow Fe(OH)^{2+} + {}^{\bullet}OH$) and the consumption ($Fe^{2+} + {}^{\bullet}OH \rightarrow Fe^{3+} + OH^-$). The dissolved iron ion has been investigated in this integrated oxidation system with TiO_2–Fe–C multi-electrode configuration when the current distribution is controlled to 1.5 mA for the carbon cathode, 0.2 mA for the TiO_2 photoanode, and 1.3 mA for Fe anode. The experimental result of electrogeneration Fe^{2+} is show in Fig. 9. Obviously, the total iron ion concentration gradually rises in the PEC reaction and eventually reaches 1.9×10^{-5} M after 180 min. No obvious precipitation of ferric hydroxide is found in the above experiment. It means that ferric/ferrous ion concentration is at a low level and the Fe^{2+} predominantly takes part in electro-Fenton oxidation

Table 3 Fitting curve formulas of the H_2O_2 concentration (*c*, mM) as a function of the electrolyzing time (*t*, min) in a Pt–C electrode pair reaction system with a current density (*I*, μA cm^{-2}) control of multiporous carbon cathode

Current density (μA cm^{-2})	20	40	80	120
Curve formulas	$c = 0.425*[1 - e^{(-0.0022*t)}]$	$c = 0.633*[1 - e^{(-0.0037*t)}]$	$c = 0.868*[1 - e^{(-0.0074*t)}]$	$c = 1.047*[1 - e^{(-0.0132*t)}]$

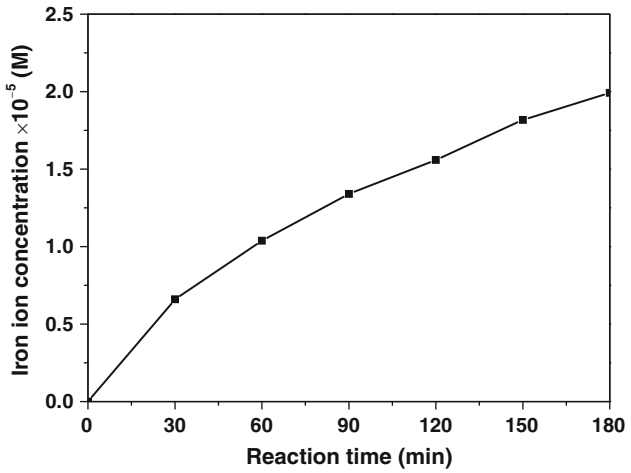

Fig. 9 Total iron ion concentration in terms of reaction time in electro-Fenton-assisted PEC process with TiO_2–Fe–C multi-electrode configuration

reaction for OG degradation. In this study, the iron sheet has been covered with a surface passive layer through an electrochemical pretreatment in nitric acid, sulfuric acid, and perchloric acid solution. Therefore, the release of ferrous ion from the passivated iron electrode can be highly restrained in comparison with raw iron sheet in the integrated PEC process. The concentration control of ferrous ion and the electrogeneration H_2O_2 will benefit the Fenton reaction in H_2O_2-assisted TiO_2 PEC process.

3.6 Individual oxidation reaction efficiency

To better understand the role of individual oxidation reaction in electro-Fenton-assisted PEC, three experiments

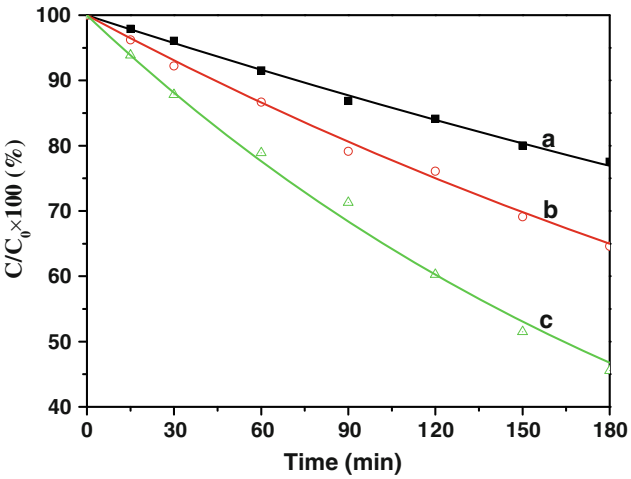

Fig. 10 OG degradation curves under UV light illumination in different electrode pair reaction system with a current control: *a* Fe–C electrode pair with 120 μA cm^{-2} for C and 150 μA cm^{-2} for Fe, *b* TiO_2–C electrode pair with 38 μA cm^{-2} for TiO_2 and 16 μA cm^{-2} for C, *c* TiO_2–C electrode pair with 300 μA cm^{-2} for TiO_2 and 120 μA cm^{-2} for C

with the designed electrode configuration are carried out. The degradation curves of OG are shown in Fig. 10. The corresponding OG degradation ratio and DOC removal ratio are summarized in Table 4.

The first experiment is conducted under UV light illumination using carbon and Fe electrodes in the absence of TiO_2 electrode. The photo-assisted electro-Fenton reaction is established with a current control of 120 μA cm^{-2} on the carbon cathode and 150 μA cm^{-2} on the Fe anode. OG degradation ratio and DOC removal ratio after 180 min are 22.5 and 12.2%, respectively (see curve a). It is believed that the electro-Fenton reaction mainly causes OG degradation. However, UV-assisted H_2O_2 photolysis reaction involved in above process has a less contribution because 365 nm UV light is less effective for H_2O_2 activation than 254 nm UV light. It should be also noted that the pH value in above experiment is around 5.8–6.1. It is not the most optimal condition for Fenton reaction that should be in the range of pH 3–4.

The other two experiments are conducted under UV light illumination using TiO_2 and carbon electrodes in the absence of Fe electrode. The H_2O_2-assisted TiO_2 PEC reaction is established. In one experiment, the TiO_2 photoanode is applied with a constant current density of 38 μA cm^{-2} and the carbon cathode is accordingly loaded with a low current density of 16 μA cm^{-2}. OG degradation ratio and DOC removal ratio after 180 min are 35.4 and 18.9%, respectively (see curve b). Herein, only a small amount of electrogeneration H_2O_2 with a cumulative concentration of 0.11 mM can be achieved at such a low current density on the carbon electrode. However, it still can promote the PEC reaction of the TiO_2 photoanode. In another experiment, the carbon cathode is applied with a constant current density of 120 μA cm^{-2} and the TiO_2 photoanode is accordingly loaded with a high current density of 300 μA cm^{-2}. OG degradation ratio and DOC removal ratio after 180 min are 54.4 and 23.8%, respectively (see curve c). In this case, OG degradation mainly involves H_2O_2-assisted PEC and anodic electrolysis oxidation reactions occurred on the TiO_2 photoanode. The electrode potential is determined to be −1.032 V for the carbon cathode and 14.492 V for the TiO_2 photoanode. The TiO_2 PEC oxidation reaction is mostly suppressed because the electrical breakdown of TiO_2 semiconductor occurs under such high potential condition. Therefore, this reaction system mainly involves anodic electrolysis oxidation reaction on the TiO_2 electrode. Although high degradation efficiency has been achieved in this experiment, comparatively low mineralization efficiency has also been found. This may indicate that OG degradation is highly affected by different mechanism of individual reaction.

It is well known that TiO_2 photocatalysis oxidation reaction of organic pollutants follows Langmuir–Hinshelwood kinetics (L–H). The first-order reaction kinetic model

Table 4 OG degradation ratio and DOC removal ratio after 180 min in different electrode pair reaction system with a current control and UV light illumination

Electrode pair system with a current control	Fe–C (C, 120 μA cm^{-2}) (Fe, 150 μA cm^{-2})	TiO_2–C (TiO_2, 38 μA cm^{-2}) (C, 16 μA cm^{-2})	TiO_2–C (TiO_2, 300 μA cm^{-2}) (C, 120 μA cm^{-2})
OG degradation ratio (%)	22.5	35.4	54.4
DOC removal ratio (%)	12.2	18.9	23.8

Table 5 Pseudo-first-order reaction rate constant (k) in different electrode pair reaction system

Reaction system	TiO_2–Fe–C (UV) (electro-Fenton-assisted PEC)	Fe–C (UV) (photo-assisted electro-Fenton)	TiO_2–C (UV) (H_2O_2-assisted PEC)	TiO_2–Pt (no UV) (anodic electrolysis)
Current distribution	TiO_2, 0.2 mA; Fe, 1.3 mA; C, 1.5 mA	C, 1.5 mA; Fe, 1.5 mA	TiO_2, 0.2 mA; C, 0.2 mA	TiO_2, 0.2 mA; Pt, 0.2 mA
k-Value	5.19×10^{-3} min^{-1}	1.46×10^{-3} min^{-1}	2.39×10^{-3} min^{-1}	0.13×10^{-3} min^{-1}

is usually used to describe TiO_2 photocatalysis and PEC reactions [28]. The experimental data can be fitted by the corresponding model equation of $c/c_0 = \exp(-k*t)$. The pseudo-first-order kinetic constant k obtained from the fitting formula can be used for the evaluation of oxidation reaction rate. The corresponding k values of both individual oxidation reaction and the integrated oxidation reaction are summarized in Table 5. The experimental result indicates that the apparent rate constant of the integrated oxidation reaction (5.19×10^{-3} min^{-1}) is even higher than the sum of three individual oxidation reactions (3.98×10^{-3} min^{-1}). The electro-Fenton-assisted PEC of independent TiO_2 long nanotube array can effectively promote OG degradation reaction. This is ascribed to the synergetic effect among these individual reactions in TiO_2–Fe–C multi-electrode system with a proper current distribution.

Microstructure modification of TiO_2, including morphology changes from microporous film structure to nanotube array, from the interconnected nanotubes to the separated ones, and from short nanotubes to long ones, can effectively improve the photocatalysis reactivity [13, 16]. Furthermore, in comparison with the previous reaction system with TiO_2–C electrode pair and the dosed ferrous ion [22], this integrated reaction system with TiO_2–Fe–C multi-electrode configuration exhibits the noticeable advantage. A proper current distribution among three functional electrodes can be achieved by means of an external resistor adjustment to keep a high cathode current on the carbon electrode and a suitable anode current on the TiO_2 photoelectrode in the same reaction system. This electro-Fenton-assisted PEC reaction system exhibits a higher efficiency than any individual oxidation reactions such as TiO_2 PEC, electro-Fenton, and anodic electrolysis oxidation reaction. This study confirms that the photoreactivity of TiO_2 nanotube array can be promoted by constructing a well-defined nanostructure of photoelectrode and introducing a functionalized multi-electrode system. Such an integrated oxidation reaction system can be developed as an efficient process for degrading environmental pollutants in practice.

4 Conclusions

Independent TiO_2 nanotube array with the separated tube wall structure has been constructed for degrading an organic pollutant. Photocatalysis and photoelectrolysis efficiency of TiO_2 nanotube array can be improved by increasing tube length from 1.1 to 6.1 μm and inter-tube space from tens to hundreds of nanometer. Furthermore, the photo-electro-assisted oxidation reaction system has been developed using TiO_2–Fe–C multi-electrode configuration with a controlled current distribution. The degradation ratio of OG can be accordingly increased from 20.4% in PEC process to 60.2% in electro-Fenton-assisted PEC process. The corresponding mineralization efficiency of OG is also improved from 8.1 to 37.4%. The apparent rate constant of 5.19×10^{-3} min^{-1} for this integrated oxidation reaction system is even higher than that of 3.98×10^{-3} min^{-1} for the sum of individual oxidation reactions including TiO_2 PEC, electro-Fenton, and anodic electrolysis. Therefore, the PEC reactivity of the TiO_2 photoelectrode can be effectively improved using independent long nanotube array as well as establishing an integrated oxidation reaction system.

Acknowledgment The study was supported by National Natural Science Foundation of China (No. 20871029), Research Fund for the Doctoral Program of Higher Education of China (No. 200802861071), Program for New Century Excellent Talents in

University of the State Ministry of Education (No. NCET-08-0119), and Southeast University Foundation (No. 4022001016 and 9207042463).

References

1. Pera-Titus M, Garcia-Molina V, Banos MA, Gimenez J, Esplugas S (2004) Appl Catal B Environ 47:219
2. Kusvuran E, Gulnaz O, Irmak S, Atanur OM, Yavuz HI, Erbatur O (2004) J Hazard Mater 109:85
3. Parsons S (2004) Advanced oxidation processes for water and wastewater treatment. IWA Publishing, London
4. Irmak S, Yavuz HI, Erbatur O (2006) Appl Catal B Environ 63:243
5. Boye B, Dieng MM, Brillas E (2003) J Electroanal Chem 557:135
6. Egerton TA, Purnama H, Purwajanti S, Zafar M (2006) J Adv Oxid Technol 9:79
7. McMurray TA, Byrne JA, Dunlop PSM, McAdams ET (2005) J Appl Electrochem 35:723
8. Shankar K, Basham JI, Allam NK, Varghese OK, Mor GK, Feng XJ, Paulose M, Seabold JA, Choi KS, Grimes CA (2009) J Phys Chem C 113:6327
9. Zhang ZH, Yuan Y, Shi GY, Fang YJ, Liang LH, Ding HC, Jin LT (2007) Environ Sci Technol 41:6259
10. Zwilling V, Darque-Ceretti E, Boutry-Forveille A, David D, Perrin MY, Aucouturier M (1999) Surf Interface Anal 27:629
11. Fadl-Allah SA, El-Sherief RM, Badawy WA (2008) J Appl Electrochem 38:1459
12. Macak JM, Tsuchiya H, Schmuki P (2005) Angew Chem Int Ed 44:2100
13. Xie YB (2006) Electrochim Acta 51:3399
14. Macak JM, Zlamal M, Krysa J, Schmuki P (2007) Small 3:300
15. Zhuang HF, Lin CJ, Lai YK, Sun L, Li J (2007) Environ Sci Technol 41:4735
16. Xie YB, Zhou LM, Lu J (2009) J Mater Sci 44:2907
17. Paramasivam I, Macak JM, Schmuki P (2008) Electrochem Commun 10:71
18. Liu Z, Zhang X, Nishimoto S, Jin M, Tryk DA, Murakami T, Fujishima A (2008) J Phys Chem C 112:253
19. Legrini O, Oliveros E, Braun AM (1993) Chem Rev 1093:671
20. Hidaka H, Shimura T, Ajisaka K, Horikoshi S, Zhao JC, Serpone N (1997) J Photochem Photobiol A Chem 109:165
21. Fernandez J, Kiwi J, Baeza J, Freer J, Lizama C, Mansilla HD (2004) Appl Catal B Environ 48:205
22. Xie YB, Li XZ (2006) Mater Chem Phys 95:39
23. Xie YB, Li XZ (2006) J Hazard Mater 138:526
24. Jovanovic VM, Hackerman N (1998) J Phys Chem B 102:9855
25. Hykrdova L, Jirkovsky J, Mailhot G, Bolte M (2002) J Photochem Photobiol A Chem 151:181
26. Zainal Z, Lee CY, Hussein MZ, Kassim A, Yusof NA (2005) J Hazard Mater 118:197
27. Quan X, Chen S, Su J, Chen JW, Chen GH (2004) Sep Purif Technol 34:73
28. Kumar KV, Porkodi K, Rocha F (2008) Catal Commun 9:82